

The contribution from rotating massive stars to the enrichment in Sr and Ba of the Milky Way

Rizzuti, F.¹, Cescutti, G.², Matteucci, F.^{1,2,3}, Chieffi, A.^{4,5}, Hirschi, R.^{6,7}, Limongi, M.^{7,8}

¹*Dipartimento di Fisica, Sezione di Astronomia, Università degli Studi di Trieste, Via Tiepolo 11, I-34143 Trieste, Italy*

²*INAF, Osservatorio Astronomico di Trieste, Via Tiepolo 11, I-34143 Trieste, Italy*

³*INFN, Trieste, Via Valerio 2, I-34127 Trieste, Italy*

⁴*INAF/IAPS, Via Fosso del Cavaliere 100, I-00133 Roma, Italy*

⁵*Monash Centre for Astrophysics (MoCA), School of Mathematical Sciences, Monash University, Victoria 3800, Australia*

⁶*Astrophysics Group, Lennard-Jones Laboratories, Keele University, Keele ST5 5BG, UK*

⁷*Kavli IPMU (WPI), The University of Tokyo, Kashiwa, Chiba 277-8583, Japan*

⁸*INAF/Osservatorio Astronomico di Roma, Via di Frascati 33, I-00040 Monte Porzio Catone, Italy*

Accepted XXX. Received YYY; in original form ZZZ

ABSTRACT

Most neutron capture elements have a double production by r- and s-processes, but the question of production sites is complex and still open. Recent studies show that including stellar rotation can have a deep impact on nucleosynthesis. We studied the evolution of Sr and Ba in the Milky Way. A chemical evolution model was employed to reproduce the Galactic enrichment. We tested two different nucleosynthesis prescriptions for s-process in massive stars, adopted from the Geneva group and the Rome group. Rotation was taken into account, studying the effects of stars without rotation or rotating with different velocities. We also tested different production sites for the r-process: magneto rotational driven supernovae and neutron star mergers. The evolution of the abundances of Sr and Ba is well reproduced. The comparison with the most recent observations shows that stellar rotation is a good assumption, but excessive velocities result in overproduction of these elements. In particular, the predicted evolution of the [Sr/Ba] ratio at low metallicity does not explain the data at best if rotation is not included. Adopting different rotational velocities for different stellar mass and metallicity better explains the observed trends. Despite the differences between the two sets of adopted stellar models, both show a better agreement with the data assuming an increase of rotational velocity toward low metallicity. Assuming different r-process sources does not alter this conclusion.

Key words: nuclear reactions, nucleosynthesis, abundances – Galaxy: evolution – Galaxy: abundances – stars: massive – stars: rotation

1 INTRODUCTION

It has been known for a long time, since Burbidge et al. (1957), that elements heavier than ⁵⁶Ni, which has the maximum binding energy per nucleon, are mostly synthesized by neutron capture. Depending on the timescale of neutron capture compared to the β decay: the slow process (s-process) when the neutron capture takes place on longer timescale, the opposite for rapid process (r-process).

Concerning the s-process, major production sites have been identified in low-mass asymptotic giant branch (AGB) stars (mass range 1.5–3.0 M_{\odot}) (Cristallo et al. 2009, 2011; Karakas 2010). AGB stars can produce all the neutron capture ele-

ments up to Pb and Bi and the main source of neutrons in this case is the reaction ¹³C(α ,n)¹⁶O. Massive stars can also produce neutron capture elements with an s-process. In massive stars, the neutron flux is weaker and is originated in this case by the reaction ²²Ne(α ,n)²⁵Mg. The s-process production is called in this case “weak s-process” and typically the lower neutron flux does not allow this process to built up very heavy elements, but only elements up to the magic number 50 such as Sr–Y–Zr. The first calculations of the 90’s (Raiteri et al. 1992) showed a strong metal dependency, and basically at metallicity lower than a tenth of the solar no production was expected. This has also been confirmed by Limongi & Chieffi (2003) on the basis of a larger grid of initial masses and metallicities. For this reason, the s-process production by massive stars at extremely

* E-mail: email

low metallicity did not have an impact in previous chemical evolution models (Travaglio et al. 1999, 2004; Cescutti et al. 2006). However, recent stellar evolution studies showed that rotation-induced mixing may keep in contact regions otherwise separate in absence of rotation. Such a phenomenon induces a peculiar nucleosynthesis as well as an increase of the nuclear burning cores, of the stellar lifetimes and of the amount of mass lost during the evolution (see Chieffi & Limongi 2013). Interesting implications are found at low metallicities, where stars are expected to be more compact and rotate faster, intensifying the effects (Meynet & Maeder 2002; Frischknecht et al. 2016, and more recently Limongi & Chieffi 2018). In terms of chemistry, one of the results of rotating mixing for massive stars is an enhancement of nitrogen and s-process production of neutron capture elements. Any investigation on the impact of this s-process production by massive stars has to deal with the production of neutron capture elements by r-process events. The r-process requires an extremely neutron-rich environment. Before the event GW170817 (Abbott et al. 2017), it was unclear where in nature the r-process can take place and several sites were proposed, and also now we cannot conclude that neutron star mergers are the only r-process events in nature (Côté et al. 2018; Simonetti et al. 2019). Core-collapse SNe or electron capture SNe were certainly the first proposed sites (Truran 1981; Cowan et al. 1991). Following theoretical studies (Arcones et al. 2007) found that these sites do not have proper entropy and neutron fraction to have an efficient r-process activation. Therefore alternative sites and mechanisms were proposed, in replacement of or in addition to SNe: neutron star mergers (NSMs) (Rosswog et al. 1999) or magneto-rotationally driven supernovae (MRD SNe) (Winteler et al. 2012; Nishimura et al. 2015).

A study of the chemical evolution enrichment adopting NSMs as source of r-process material have been carried on by Matteucci et al. (2014) (so before the NSM event GW170817 observed by LIGO and Virgo (Abbott et al. 2017)). The conclusions were that NSMs may be responsible for the r-process enrichment in the Galactic halo either totally or just in part, in a mixed scenario with both SNe II and NSMs, providing a very short time-scale for the merging after the formation of the neutron star binary (see also Argast et al. 2004; Cescutti et al. 2015; Simonetti et al. 2019). Similar studies by means of chemical evolution models have been carried on for MRD SNe by Cescutti & Chiappini (2014), whereas in Cescutti et al. (2013) the EC SNe scenario was investigated. Cescutti et al. (2013), Cescutti & Chiappini (2014), Cescutti et al. (2015) were the first studies showing that s-process driven by rotation in massive stars has a fundamental role for chemical evolution results. Independently by the r-process event considered, the s-process production by massive stars was shown to be a possible solution to explain a signature in neutron capture elements in the Galactic halo: the spread in light (e.g. Sr-Y-Zr) to heavy neutron capture elements (e.g. La, Ba). These results were obtained adopting a nucleosynthesis based on Frischknecht et al. (2012, 2016). More recently, Prantzos et al. (2018) obtained similar results, but using the theoretical nucleosynthesis obtained by Limongi & Chieffi (2018).

The main purpose of this paper consists in testing and comparing nucleosynthesis prescriptions for rotating massive stars using these two studies, Frischknecht et al. (2016) and

Limongi & Chieffi (2018). The aim is to analyse the effects produced by prescriptions coming from different assumptions on stellar evolution. Concerning the r-process component, we assume two scenarios, the MRD SNe scenario using the prescriptions obtained thanks to chemical evolution models by Cescutti & Chiappini (2014) and NSMs using the prescriptions from Matteucci et al. (2014). The tool we use for this study is a chemical evolution model of the Galaxy, based on the two-infall model Chiappini et al. (1997). The resulting abundances of elements - we will focus on Sr and Ba - as functions of metallicity are compared to the observations, to verify if the prescriptions assumed reproduce the data correctly, and if different works show compatible results. The paper is organized as follows: in Section 2 we describe the adopted observational data. In Section 3 the chemical evolution model is presented. In Section 4 the adopted nucleosynthesis prescriptions are discussed. In Section 5 the results are presented and in Section 6 some conclusions are drawn.

2 OBSERVATIONAL DATA

Three main sources of chemical abundances of Galactic stars were adopted. For low metallicities ($[\text{Fe}/\text{H}]$ from -4 to -1) Milky Way halo stars abundances were taken from various authors (JINA-CEE database). The totality of the authors is displayed in Table 1.

Another sample, from Battistini & Bensby (2016), was used for the data belonging to the thin and thick disks of the Milky Way. In their paper, the original data from Bensby et al. (2014) were extended to include also the abundances of neutron capture elements.

Finally, the data of the halo star TYC 8442-1036-1 from the work of Cescutti et al. (2016) were taken into account ($[\text{Fe}/\text{H}] = -3.5$).

All the authors normalized the data according to solar abundances taken from Asplund et al. (2009).

3 THE CHEMICAL EVOLUTION MODEL

The model employed reproduces the evolution of the Galaxy, assuming one main infall episode. It is based on the two-infall model Chiappini et al. (1997), but it has only one single infall. The choice of a sequential one-infall model is based on the consideration that the main difference with the two-infall model is the gap in star formation at the end of the halo-thick disk phase, which is not yet proven observationally. On the other hand, the main behavior of the abundance ratios as functions of $[\text{Fe}/\text{H}]$ is very similar. Moreover, here we do not distinguish between thick and thin disk stars. The adopted model is a homogeneous one, namely it assumes instantaneous mixing approximation: the gas mixing time is considered smaller than the timestep of integration, so the ISM is well mixed at all times. The values are calculated for one zone, the solar vicinity. We assume the age of the Milky Way to be 14 Gyr.

The equations which rule the gas fraction G_i of a certain

Table 1. Sources for observational data abundances.

	Ba	Sr		Ba	Sr
Aoki et al. (2002)	X	X	Ivans et al. (2003)	X	X
Aoki et al. (2005)	X	X	Ivans et al. (2006)	X	X
Aoki et al. (2007a)	X	X	Jacobson et al. (2015)	X	X
Aoki et al. (2007b)	X		Johnson (2002)	X	X
Aoki et al. (2008)	X	X	Jonsell et al. (2005)	X	
Aoki et al. (2012)	X		Lai et al. (2007)	X	X
Aoki et al. (2013)	X	X	Lai et al. (2008)	X	X
Aoki et al. (2014)	X	X	Li et al. (2015a)	X	X
Barklem et al. (2005)	X	X	Li et al. (2015b)	X	X
Battistini & Bensby (2016)	X	X	Mashonkina et al. (2010)	X	X
Bensby et al. (2011)	X		Mashonkina et al. (2014)	X	X
Bonifacio et al. (2009)	X	X	Masseron et al. (2006)	X	X
Burris et al. (2000)	X	X	Masseron et al. (2012)	X	
Caffau et al. (2011)	X	X	McWilliam et al. (1995)	X	X
Carretta et al. (2002)	X	X	Norris et al. (1997a)	X	X
Cayrel et al. (2004)	X	X	Norris et al. (1997b)	X	X
Cescutti et al. (2016)	X	X	Norris et al. (1997c)	X	X
Christlieb et al. (2004)	X	X	Placco et al. (2014)	X	X
Cohen et al. (2004)	X	X	Placco et al. (2015)	X	X
Cohen et al. (2013)	X	X	Preston & Sneden (2000)	X	X
Cowan et al. (2002)	X	X	Preston et al. (2006)	X	X
Frebel et al. (2007)	X		Roederer et al. (2010)	X	X
Fulbright (2000)	X		Roederer et al. (2014)	X	X
Hansen et al. (2012)	X	X	Ryan et al. (1991)	X	X
Hansen et al. (2015)	X	X	Ryan et al. (1996)	X	X
Hayek et al. (2009)	X	X	Siqueira Mello et al. (2014)	X	X
Hollek et al. (2011)	X	X	Spite et al. (2014)	X	X
Honda et al. (2004)	X	X	Westin et al. (2000)	X	X
Honda et al. (2011)	X	X	Yong et al. (2013)	X	X
Ishigaki et al. (2010)	X		Zhang et al. (2009)	X	
Ishigaki et al. (2013)	X	X			

element i are the following:

$$\begin{aligned}
 \dot{G}_i(r_\odot, t) = & -\psi(r_\odot, t) X_i(r_\odot, t) \\
 & + \int_{M_L}^{M_{Bm}} \psi(r_\odot, t - \tau_m) Q_{mi}(t - \tau_m) \phi(m) dm \\
 & + A \int_{M_{Bm}}^{M_{BM}} \phi(m) \cdot \left[\int_{\mu_m}^{0.5} f(\mu) \psi(r_\odot, t - \tau_{m2}) Q_{mi}(t - \tau_{m2}) d\mu \right] dm \\
 & + (1 - A) \int_{M_{Bm}}^{M_{BM}} \psi(r_\odot, t - \tau_m) Q_{mi}(t - \tau_m) \phi(m) dm \\
 & + \int_{M_{BM}}^{M_U} \psi(r_\odot, t - \tau_m) Q_{mi}(t - \tau_m) \phi(m) dm \\
 & + \dot{G}_i(r_\odot, t)_{inf}
 \end{aligned} \tag{1}$$

where the first term on the right-hand side represents the gas subtracted by the ISM and locked into stars, the integrals refer to the production and restitution of the element i from the stars into the ISM, and the last term is the gas accretion rate. In particular, X_i is the abundance by mass of the element i , Q_{mi} the fraction of mass restored by a star of the mass m in the form of the element i , $f(\mu)$ the distribu-

tion of the mass ratio for the secondary in a binary system giving use to SNe Ia, $\phi(m)$ the initial mass function (IMF), which here is the one suggested by [Scalo \(1986\)](#).

The star formation rate (SFR) $\psi(r, t)$ is expressed as:

$$\psi(r, t) = \nu \left(\frac{\Sigma(r, t_G)}{\Sigma(r, t)} \right)^{k-1} G_{gas}^k(r, t) \tag{2}$$

where ν is the star formation efficiency, here 1.2 Gyr^{-1} , $\Sigma(r, t)$ the total surface mass density, $t_G = 14 \text{ Gyr}$ the age assumed for the Milky Way, $k = 1.4$ the law index, and $G_{gas}(r, t)$ the surface density normalized to the present time total surface mass density in the disk. The equation is the same as in [Chiappini et al. \(1997\)](#), but the ratio $(\Sigma(r, t)/\Sigma(r_\odot, t))^{2k+1}$ in the original formula, namely the total surface mass density over the total surface mass density at the solar position, is set equal to 1 for we are in the solar neighborhood.

The four integrals have different meanings:

(i) the first represents the stars in the mass range M_L ($0.8 M_\odot$, the lower mass limit) to M_{Bm} ($3 M_\odot$) with a lifetime of τ_m ;

(ii) the second represents the SNe Ia originating from white dwarfs - binary systems, from the minimum M_{Bm} ($3 M_\odot$) to the maximum M_{BM} ($16 M_\odot$) allowed for the whole binary systems, the parameter $A = 0.05$ being the fraction of binary systems with the right characteristics to give rise to SNe Ia ([Matteucci & Recchi 2001](#)), and τ_{m2} the lifetime of the secondary star;

(iii) the third describes the single stars with masses in the range M_{Bm} to M_{BM} , which can end their lives either as white dwarfs (3-9 M_{\odot}) or as core collapse SNe (9-16 M_{\odot});

(iv) the fourth represents the core collapse SNe, from the minimum mass M_{BM} to the maximum one M_U (100 M_{\odot} , the upper mass limit).

Finally, for the gas infall the following law is adopted:

$$\dot{G}_i(r, t)_{inf} = a(r) (X_i)_{inf} e^{-t/\tau(r)} \quad (3)$$

where the parameter $a(r)$ is the total surface mass density at the present time, fixed to 65 $M_{\odot} pc^{-2}$, $(X_i)_{inf}$ are the abundances for the infalling material, assumed to be primordial, and $\tau(r)$ the characteristic time of formation for the disk, which in the solar neighbourhood is $\tau(8 kpc) = 7$ Gyr (Chiappini et al. 1997).

4 NUCLEOSYNTHESIS PRESCRIPTIONS

As reported in the Introduction, most of the neutron capture elements have a double production and are formed both by r-process and s-process. This is the case of barium and strontium, the two elements analysed in this work. The duality of production for barium has been studied in chemical evolution models since Travaglio et al. (1999) and Cescutti et al. (2006), showing that Ba has a main s-process component produced by low mass AGB stars but also an r-process production. Here we assume also the s-process contribution from massive stars, taking into account the rotational velocity and stellar metallicity as initial parameters. This has already been considered in Cescutti et al. (2013), Cescutti & Chiappini (2014), Cescutti et al. (2015), Prantzos et al. (2018) but here we compare for the first time two nucleosynthesis sets (Frischknecht et al. 2016; Limongi & Chieffi 2018) for rotating massive stars.

The set of nucleosynthesis for different sources of neutron capture elements is rather complex and was taken from different authors; we have summarized them in Table 2.

Low mass stars, in a mass range of 1.3-3 M_{\odot} , which are responsible for part of the s-process, were taken from Cristallo et al. (2009, 2011). We used results from models of non-rotating stars. However, these non-rotating yields tend to overproduce the neutron capture elements at solar abundance. On the other hand, rotating yields produce significantly lower amount of neutron capture elements. For this reason, we decided to divide by a factor of two the non-rotating yields, since rotational yields would have produced a similar decrease.

For the s-process component in rotating massive stars, we have decided to investigate two available dataset, Frischknecht et al. (2016) and Limongi & Chieffi (2018).

Frischknecht et al. (2016) studied the impact of rotation in massive stars nucleosynthesis; they produced a large grid of yields using several models with different features. They took into account a stellar mass range of 15-40 M_{\odot} ; the stars are assumed to have different initial rotational velocities, selected by mass and metallicity. Four metallicities, expressed in $[Fe/H]$, are explored: 0, -1.8, -3.8 and -5.8. In our model we considered only the first three metallicities. For the lowest metallicity (i.e. $[Fe/H] = -5.8$), only a model of 25 M_{\odot} has been computed, and for this reason we decide not to extrapolate the results. Instead, we assumed the yields from

$[Fe/H] = -3.8$ also for lower metallicities.

For rotational scenarios in the first two metallicities $[Fe/H] = 0$ and -1.8 , we used the models for which Frischknecht et al. (2016) fixed the value of standard initial rotation rate over critical velocity to $v_{ini}/v_{crit} = 0.4$. With this parameter assumed as a constant, the resulting average equatorial rotation velocity on the MS, $\langle v \rangle_{MS}$, increases with decreasing metallicity; for 15-20 M_{\odot} stars at solar metallicity, $\langle v \rangle_{MS}$ corresponds to 200-220 km/s.

For the metallicity $[Fe/H] = -3.8$, in order to include a stronger production of s-process, we decided to use the model providing a faster rotation ($v_{ini}/v_{crit} = 0.5$) and a lower $^{17}O(\alpha, \gamma)$ rate (one tenth of the standard choice, i.e. Caughlan & Fowler 1988). Since the only model produced by Frischknecht et al. (2016) with such assumptions is for a stellar mass of 25 M_{\odot} , we decided to compute for each element a ratio between the yields obtained from the fast rotator model and the previous one at 25 M_{\odot} , and then apply the resulting scale factors to the other models with metallicity $[Fe/H] = -3.8$ and masses 15, 20 and 40 M_{\odot} (see Cescutti et al. 2013).

The models developed by Frischknecht et al. (2016) and their characteristics are reported in Table 3. Notice that, of the original models, we used only the ones with rotation.

The work of Limongi & Chieffi (2018) also produced new nucleosynthesis models of massive stars, but with different assumptions. They considered a larger stellar mass range of 13-120 M_{\odot} , and four metallicities: $[Fe/H] = 0, -1, -2$ and -3 . They produced a set of yields for stars with three possible velocities, using an initial speed of 0 km/s (non rotating), 150 km/s and 300 km/s. We decided here to develop three models assuming all stars rotate with the same initial speed. Realistically, a velocity distribution is expected for stellar rotation, but our assumption allows us to investigate a mean velocity.

Another important difference between the two papers is that in Limongi & Chieffi (2018) the models have been computed up to the pre-SN stage, and the explosive nucleosynthesis has been taken into account by means of induced explosions, while Frischknecht et al. (2016) models stop at the beginning of the O-core burning. In the model we use, for Limongi & Chieffi (2018) the amount of matter that effectively is ejected is the one lost by the star by stellar wind, during the pre-SN evolution, plus the one ejected during the explosion. The mass cut between the collapsing core and the ejected envelope has been fixed in such a way that the ejecta contains 0.07 M_{\odot} of ^{56}Ni , a typical value observed in the spectra of core-collapse SNe. In particular, from the Limongi & Chieffi (2018) sets developed for this scenario, we used here the Set F, where each mass is considered to eject 0.07 M_{\odot} of ^{56}Ni .

A comparison between the models of the two works can be seen in Figure 1.

Also for the r-process events, we investigate two scenarios. In the first, MRD SNe are taken into account as r-process events, as suggested in Winteler et al. (2012) and later confirmed by Nishimura et al. (2015). In this case, we used the assumptions adopted in Cescutti & Chiappini (2014), where 10% of all the stars in the range 10-80 M_{\odot} are considered productive, with a timescale of 3-25 Myr. In the second, we study the possibility of using NSMs instead of MRD SNe as r-production sites (Rosswog et al. 1999). In this case, the

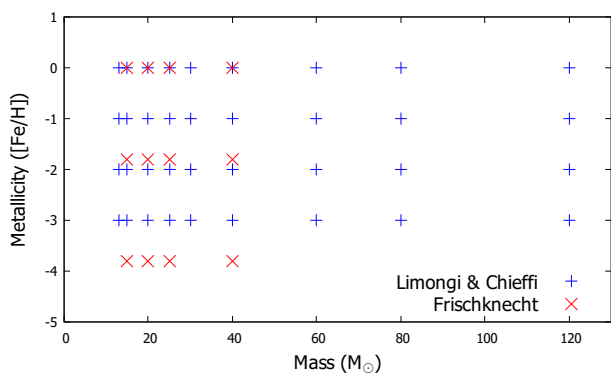
Table 2. Authors used for nucleosynthesis prescriptions.

	s-process	r-process
Low mass stars	Cristallo et al. (2009, 2011)	—
Massive stars	Frischknecht et al. (2016) Limongi & Chieffi (2018)	Rosswog et al. (1999) Winteler et al. (2012)
NSM	—	Matteucci et al. (2014) Cescutti et al. (2015)

Table 3. Model parameters adopted for our work from Frisknecht et al. (2016): initial mass, model label, initial ratio of surface velocity to critical velocity, time-averaged surface velocity during the MS phase, metallicity.

Mass (M_{\odot})	Model	$v_{\text{ini}}/v_{\text{crit}}$	$\langle v \rangle_{\text{MS}}$ (km/s)	[Fe/H]
15	A15s4	0.4	200	0.0
	B15s4	0.4	234	-1.8
	C15s4	0.4	277	-3.8
20	A20s4	0.4	216	0.0
	B20s4	0.4	260	-1.8
	C20s4	0.4	305	-3.8
25	A25s4	0.4	214	0.0
	B25s4	0.4	285	-1.8
	C25s4	0.4	333	-3.8
	C25s5b ^a	0.5	428	-3.8
40	A40s4	0.4	186	0.0
	B40s4	0.4	334	-1.8
	C40s4	0.4	409	-3.8

^a Models calculated with a lower $^{17}\text{O}(\alpha, \gamma)$.


Figure 1. The two papers used for rotating massive stars Limongi & Chieffi (2018) (blue crosses) and Frisknecht et al. (2016) (red crosses) compared for mass and metallicity employed in the models.

rate and the yields were adopted from the work of Matteucci et al. (2014) and Cescutti et al. (2015) respectively. They suggest that r-element material can be produced only by NSMs if the neutron stars originate in the stellar mass range of 9-50 M_{\odot} , the coalescence timescale is fixed and equal to 1 Myr and the rate of NSM events is 0.018, the one of Kalogera et al. (2004). The recent observations of the LIGO/Virgo rate for the event GW170817 seem to confirm

this result (Matteucci et al. 2018). In both r-process cases, the adopted scaling factor between Sr and Ba has been taken from the solar system r-process contribution as determined by Simmerer et al. (2004). This simple approach is reasonable, since the emphasis of this paper is not on the r-process issue but on the contribution from rotating massive stars to the production of strontium and barium.

Finally, concerning the iron yields from core-collapse SNe, we decided to adopt the ones from Kobayashi et al. (2006), the same used by Matteucci et al. (2014), instead of the ones from Limongi & Chieffi (2018). The reason for this choice is that the two works approach very similar results, as we chose to be consistent with Matteucci et al. (2014).

5 RESULTS

5.1 Ratios of heavy elements

We present here the ratios for [Ba/Fe], [Sr/Fe] and [Sr/Ba]. The reason for this choice is to study the trends of production for strontium and barium as representative respectively of the first and second peak of the s-process production. Moreover, the behaviour of [Sr/Ba] can provide a differential information about the production of these elements by the s-process in rotating massive stars, that is the focus of the present work.

In order to make the trend of the data clearer, the metallicity range has been divided into equal sections; for each one, a mean value of abundance for observational data has been computed. For every mean dot an error has been associated, estimated as standard deviation; the set of error bars delimits a grey shadowed area which we consider the acceptable zone.

We run the models using the prescriptions described in Section 4. The models we developed and their features are summarized in Table 4.

First we present the results obtained with MRD SNe as r-process sites. The ratio of [Ba/Fe] versus [Fe/H] is shown in Figure 2. The dots represent the observational data: for them, a black mean trend is tracked. The red line is model F+MRD with Frisknecht et al. (2016) yields, the blue lines are relative to models LC000+MRD (solid), LC150+MRD (dashed) and LC300+MRD (double dashed), using Limongi & Chieffi (2018) yields assuming all stars rotate with the same initial velocity 0 km/s, 150 km/s and 300 km/s respectively.

As for the two prescriptions, we can see that the results obtained with the use of the F, LC000 and LC150 set of yields cover properly the data in every range of metallicity; the use

Table 4. The models and their prescriptions.

Model name	s-process in rotating massive stars	Assumed stellar rotational velocity	r-process
F+MRD	Frischknecht et al. (2016)	see Table 3	Rosswog et al. (1999) ; Winteler et al. (2012)
LC000+MRD	Limongi & Chieffi (2018)	non rotating	Rosswog et al. (1999) ; Winteler et al. (2012)
LC150+MRD	Limongi & Chieffi (2018)	150 km/s	Rosswog et al. (1999) ; Winteler et al. (2012)
LC300+MRD	Limongi & Chieffi (2018)	300 km/s	Rosswog et al. (1999) ; Winteler et al. (2012)
LC075+MRD	Limongi & Chieffi (2018)	75 km/s ^a	Rosswog et al. (1999) ; Winteler et al. (2012)
LC225+MRD	Limongi & Chieffi (2018)	225 km/s ^a	Rosswog et al. (1999) ; Winteler et al. (2012)
F+NSM	Frischknecht et al. (2016)	see Table 3	Matteucci et al. (2014) ; Cescutti et al. (2015)
LC000+NSM	Limongi & Chieffi (2018)	non rotating	Matteucci et al. (2014) ; Cescutti et al. (2015)
LC150+NSM	Limongi & Chieffi (2018)	150 km/s	Matteucci et al. (2014) ; Cescutti et al. (2015)
LC300+NSM	Limongi & Chieffi (2018)	300 km/s	Matteucci et al. (2014) ; Cescutti et al. (2015)

^a Yields obtained by interpolation process: see Section 5.2

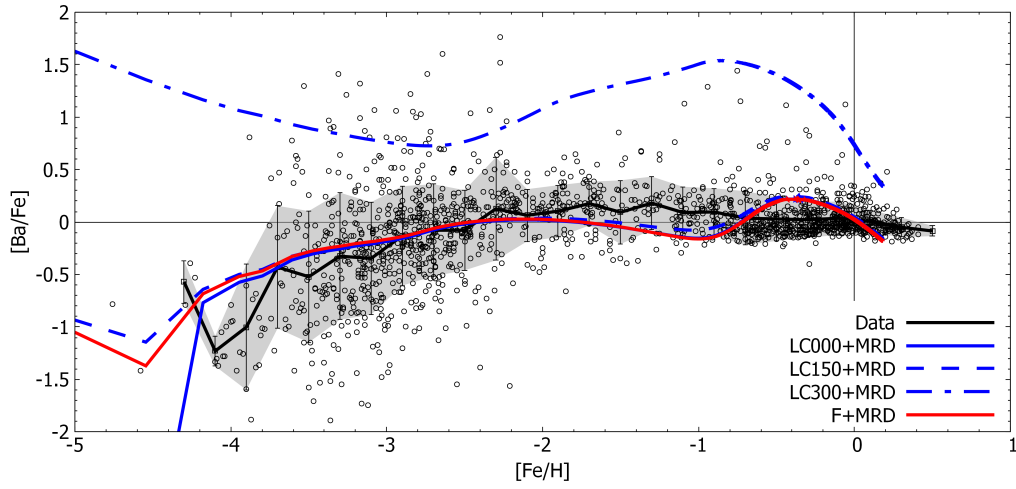


Figure 2. $[\text{Ba}/\text{Fe}]$ versus $[\text{Fe}/\text{H}]$. The black dots, track and shadowed area are the observations (sources listed in Table 1); red line is model F+MRD; blue solid line is model LC000+MRD; blue dashed line is model LC150+MRD; blue double dashed line is model LC300+MRD (see Table 4).

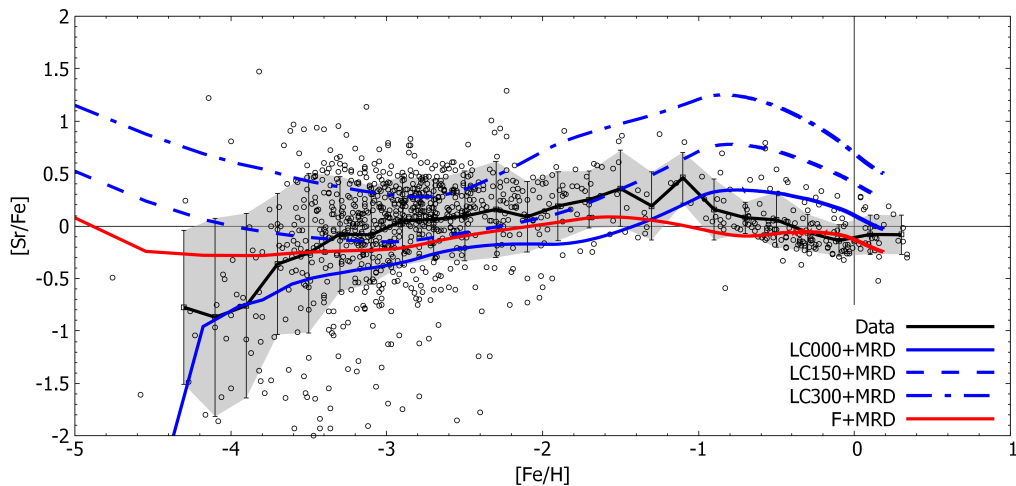


Figure 3. $[\text{Sr}/\text{Fe}]$ versus $[\text{Fe}/\text{H}]$. The black dots, track and shadowed area are the observations (sources listed in Table 1); red line is model F+MRD; blue solid line is model LC000+MRD; blue dashed line is model LC150+MRD; blue double dashed line is model LC300+MRD (see Table 4).

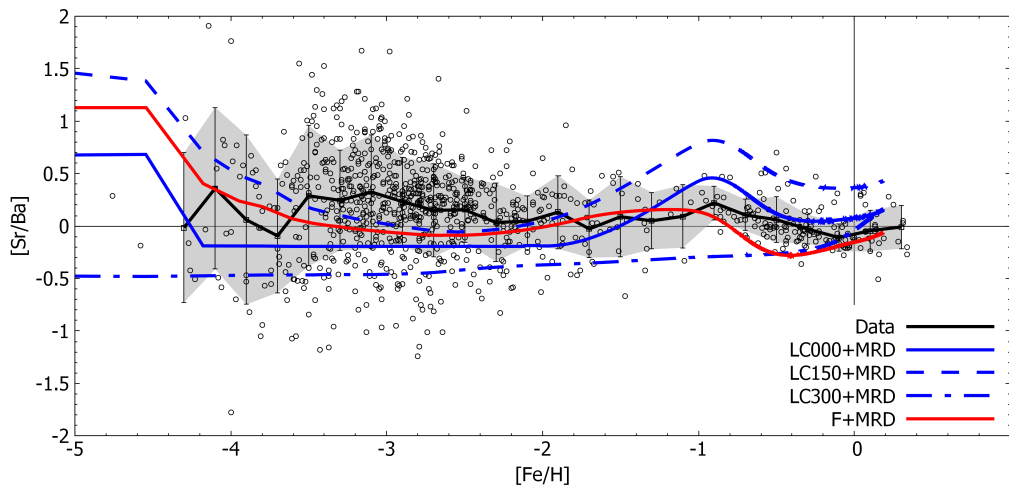


Figure 4. $[\text{Sr}/\text{Ba}]$ versus $[\text{Fe}/\text{H}]$. The black dots, track and shadowed area are the observations (sources listed in Table 1); red line is model F+MRD; blue solid line is model LC000+MRD; blue dashed line is model LC150+MRD; blue double dashed line is model LC300+MRD (see Table 4).

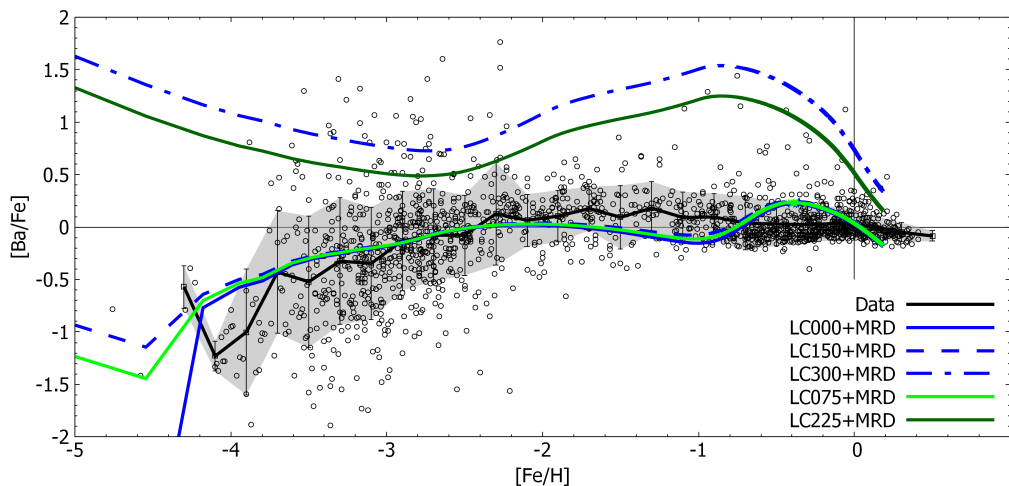


Figure 5. $[\text{Ba}/\text{Fe}]$ versus $[\text{Fe}/\text{H}]$. The black dots, track and shadowed area are the observations (sources listed in Table 1); blue solid line is model LC000+MRD; blue dashed line is model LC150+MRD; blue double dashed line is model LC300+MRD; light green line is model LC075+MRD; dark green line is model LC225+MRD (see Table 4).

of the LC300 yields, on the contrary, produce an amount of barium that is not compatible with the observations. The reason for this result is that barium is mostly produced by r-process in our framework, so in the case of extremely high production by s-process, our model is not compatible with the data.

We recall that the s-process from AGB stars has a long timescale, so in the earliest stages its production is not significant. We still have the s-process from rotating massive stars, but such a contribution is in general lower than the one from the r-process.

Around $[\text{Fe}/\text{H}] = -1$, the contribution for barium by AGB stars starts to be effective; its effect balances the production of iron by SNe Ia: the resulting trend is almost flat.

We can observe a decline also toward metallicities higher than solar. The recent work by Prantzos et al. (2018) predict this behaviour for barium and the second peak s-elements too; the chemical abundances of stars with super solar metal-

licity show a decline too, but less extreme than model predictions.

Similar results can be found for the $[\text{Sr}/\text{Fe}]$ ratio, reported in Figure 3. F, LC000 and LC150 yields match remarkably well the data. On the other hand, we found that the results of the model with all stars rotating at the highest velocity (LC300) overproduce the ratio of $[\text{Sr}/\text{Fe}]$. A light decline toward metallicities higher than solar is seen but, unlike the previous case, observations do not show such a trend for strontium. For strontium all the models with rotations by Limongi & Chieffi (2018) overestimate the solar abundance, contrary to barium models.

Finally, the key ratio - $[\text{Sr}/\text{Ba}]$ - is presented in Figure 4. For this ratio, the chemical abundances of stars at $-4 < [\text{Fe}/\text{H}] < -3$ are on average (black line) higher than the $[\text{Sr}/\text{Ba}]$ ratio by r-process only. For the r-process contribution only, we can compare to model LC000+MRD at these metallicities, which is almost exclusively r-process; in fact with no rota-

tion, there is no s-process production of Sr and Ba. We also note that for $[\text{Fe}/\text{H}] < -4$, it is difficult to claim any clear trend, given also the scarce number of data.

For this plot, assuming the low velocity yields (150 km/s) from [Limongi & Chieffi \(2018\)](#) for all stars returns the most accurate trend which satisfies the observations. As we said in Sec 4, this is an extreme assumption, for it does not allow us to appreciate the full distribution of velocities. The non-rotating yields or the high velocity ones represent extremities of such distribution; there are certainly some stars which possess these features, but the data tell they are not frequent. The reasons for this behaviour are different: in the first case of no rotation, with no production by s-process, the r-process enrichment do not fit the data; in the second of high speed rotation, the model produces too much Ba compared to Sr.

On the other hand, the low velocity set displays the best behaviour compared to the data, although possibly the high value of $[\text{Sr}/\text{Ba}]$ in the model is present at $[\text{Fe}/\text{H}] \sim -4$, with a 0.5 dex displacement compared to the data at $[\text{Fe}/\text{H}] \sim -3.5$. This can be due to the single chemical evolution model that we use to interpret the data from the Galactic halo to the solar metallicity. At this low metallicity the model obtained using the nucleosynthesis computed in [Frischknecht et al. \(2016\)](#) performed similarly to the model assuming 150 km/s from [Limongi & Chieffi \(2018\)](#). We interpret this due to the s-process contribution of rotating massive stars that was also the main conclusion in [Cescutti et al. \(2013\)](#), that was based only on the yields by [Frischknecht et al. \(2012\)](#).

5.2 Velocity interpolation

Considering the results of the previous section 5.1, we decided to investigate rotational velocities intermediate between those in the grid proposed by [Limongi & Chieffi \(2018\)](#). We used a linear interpolation over mass and metallicity on two prescriptions different in stellar speed, to obtain a new set with intermediate features, which we denoted by the arithmetic mean velocity. Two interpolations had been produced: 75 km/s between the sets 0 and 150 km/s (model LC075+MRD), and 225 km/s between 150 and 300 km/s (model LC225+MRD).

The results of such method for $[\text{Ba}/\text{Fe}]$, $[\text{Sr}/\text{Fe}]$ and $[\text{Sr}/\text{Ba}]$ are displayed in Figure 5, 6, and 7 respectively, with a light green line for model LC075+MRD and a dark green one for model LC225+MRD, compared with the original blue models LC000+MRD, LC150+MRD and LC300+MRD. The new trends are, as we expected, intermediate between the original tracks.

A comparison between models is useful to determine which velocity better covers different scenarios: we can identify the best-fitting model for a range of metallicity, therefore the rotational velocity of most stars in that range.

In particular, from the $[\text{Sr}/\text{Fe}]$ and $[\text{Sr}/\text{Ba}]$ behaviour, we can see that up to $[\text{Fe}/\text{H}] = -2$, the mean velocity which best covers the data is 150 km/s; from $[\text{Fe}/\text{H}] = -2$ to -1 , a transition to 75 km/s can be seen, while for $[\text{Fe}/\text{H}] > -1$ the non rotating assumption is preferred.

In [Prantzos et al. \(2018\)](#), where we recall the same [Limongi & Chieffi \(2018\)](#) data were used, a similar assumption was made: the initial velocity of massive stars is on average about 180 km/s up to $[\text{Fe}/\text{H}] = -3$, then it decreases until reaching a plateau of 50 km/s at solar metallicities. As we can see, our predicted velocities are in general lower.

5.2.1 A mixed model

In Section 5.1, from the study on $[\text{Sr}/\text{Ba}]$ ratio at low metallicities, the scenario provided by [Limongi & Chieffi \(2018\)](#) indicates that non-rotating stars cannot explain the chemical abundances in the Galactic halo around $[\text{Fe}/\text{H}] = -3$, but the best fit of the data assumes stars having on average the low velocity 150 km/s or the interpolation 75 km/s. On the other hand, the non-rotating case fits the data at solar metallicities quite well, while the model with rotation at 150 km/s (as well as the model at 75 km/s) predicts a trend with a too high $[\text{Sr}/\text{Ba}]$ ratio compared to the data. We can conclude that a good fit could be produced by a model using the rotating [Limongi & Chieffi \(2018\)](#) prescriptions for low metallicities up to $[\text{Fe}/\text{H}] \sim -2$, and the non-rotating ones at higher metallicities.

Such a hypothesis is in agreement with the assumptions taken by the Geneve group ([Meynet et al. 2006](#); [Hirschi 2007](#)) and adopted also by [Frischknecht et al. \(2016\)](#). They assume in fact a constant ratio between initial velocity and critical velocity. This produces automatically an higher velocity for models at low metallicity, as we reported in Section 4 (see Table 3).

As we noticed, the same conclusion has been suggested within the paper of [Prantzos et al. \(2018\)](#), but they based their constraint on nitrogen trend.

Assuming no rotation (or low rotational velocity, below 75

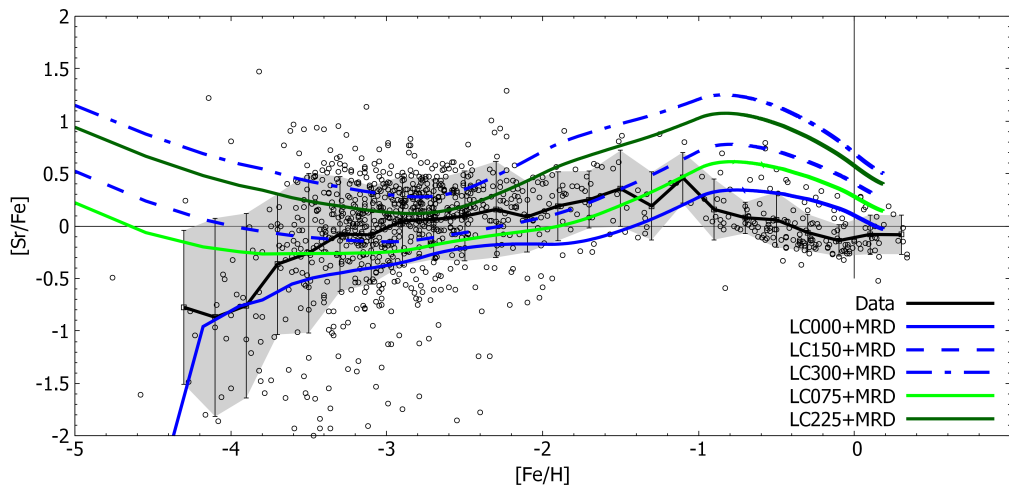


Figure 6. $[\text{Sr}/\text{Fe}]$ versus $[\text{Fe}/\text{H}]$. The black dots, track and shadowed area are the observations (sources listed in Table 1); blue solid line is model LC000+MRD; blue dashed line is model LC150+MRD; blue double dashed line is model LC300+MRD; light green line is model LC075+MRD; dark green line is model LC225+MRD (see Table 4).

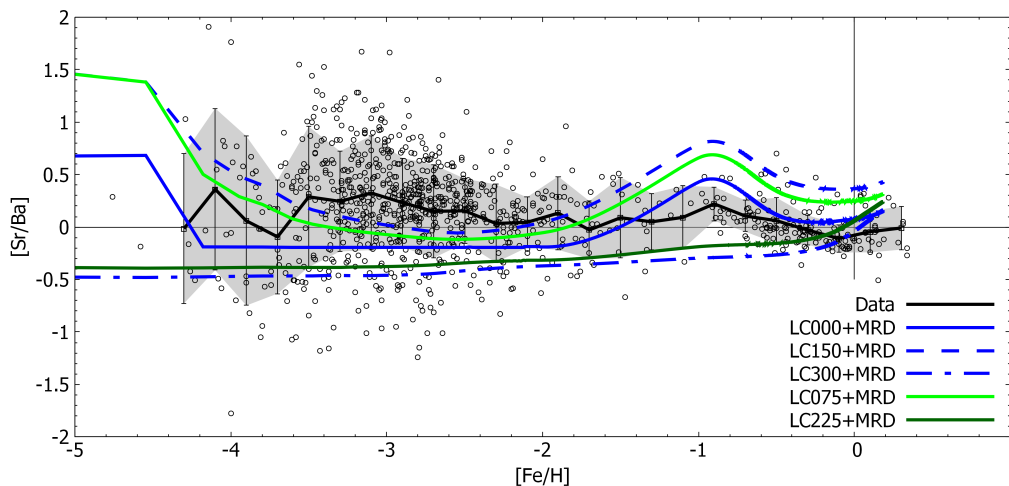


Figure 7. $[\text{Sr}/\text{Ba}]$ versus $[\text{Fe}/\text{H}]$. The black dots, track and shadowed area are the observations (sources listed in Table 1); blue solid line is model LC000+MRD; blue dashed line is model LC150+MRD; blue double dashed line is model LC300+MRD; light green line is model LC075+MRD; dark green line is model LC225+MRD (see Table 4).

km/s) is a specific result of our models LC. For example, in the results considering yields from Frischknecht et al. (2016) (see Table 3), a minimum rotation is still assumed (and required) to explain observations at best.

Moreover, this outcome is driven only by considering neutron capture elements; indeed, for nitrogen, Prantzos et al. (2018) obtained slightly different constraints.

5.3 Neutron star mergers and time delay

We decided to verify the impact of using NSMs as r-process sites instead of MRD SNe. For this test, we need also to assume a coalescence timescale for the NSMs. We investigate these timescales: $\tau = 0, 1, 10$ or 100 Myr. In this model we assume that the Ba and Sr fractions which originate from the r-process are formed in NSMs; in particular, the yield of Ba and Sr are obtained by scaling the Eu contribution according to the abundance ratios observed in solar abun-

dance (see also Sect. 4)

In Fig. 8, we present the models F+NSM using Frischknecht et al. (2016) yields for massive star s-process and NSMs for r-process: the trends, for different NSM time-delays, are in purple (with longer τ presented with lighter shades); in red, model F+MRD with Frischknecht et al. (2016) yields and MRD SNe. From Fig. 8, it is evident that the best choice for the coalescence timescale is the shortest timescale: $\tau = 1$ Myr. It is also noticeable that using Frischknecht et al. (2016) yields and NSMs for $\tau = 0$ or 1 Myr is very similar to the previous model with MRD SNe.

An extensive analysis of the best choice for the delay time can be found in Matteucci et al. (2014) and Cescutti et al. (2015); also these works conclude that NSMs with a coalescence timescale of 1 Myr can be a reasonable scenario concerning the europium production in the Galaxy.

Also Limongi & Chieffi (2018) yields has been tested together with NSMs: Figs 9 and 10 display the modified

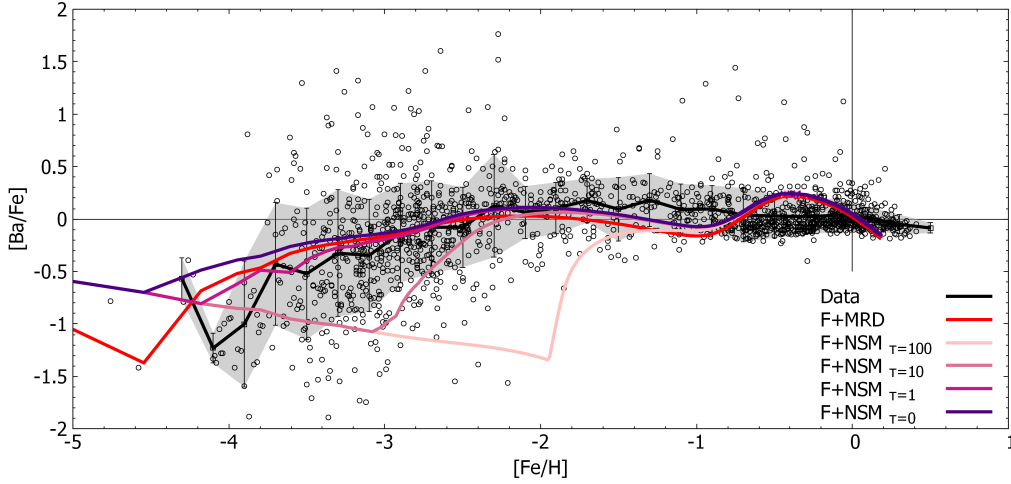


Figure 8. $[\text{Ba}/\text{Fe}]$ versus $[\text{Fe}/\text{H}]$. The black dots, track and shadowed area are the observations (sources listed in Table 1); red line is model F+MRD; purple lines are model F+NSM with variations in the time delay, namely (from darker to lighter) $\tau = 0, 1, 10, 100$ Myr (see Table 4).

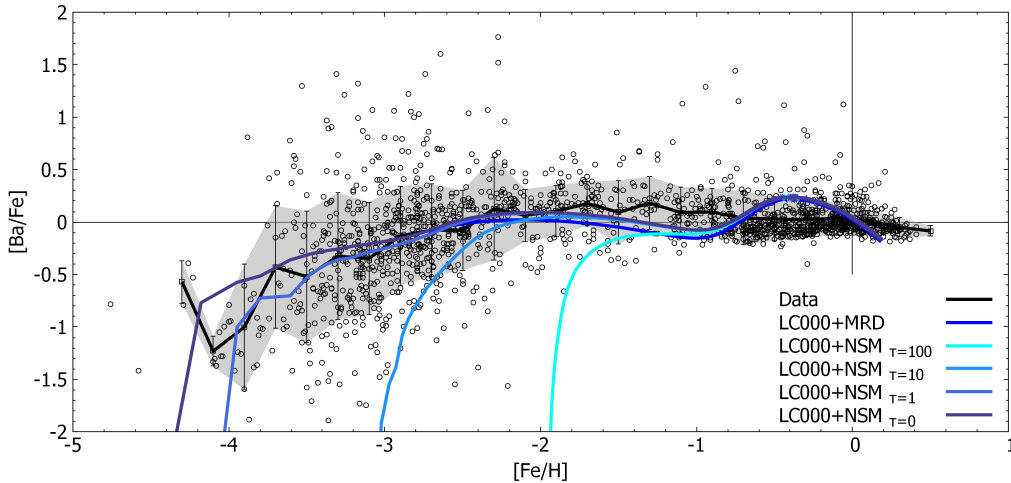


Figure 9. $[\text{Ba}/\text{Fe}]$ versus $[\text{Fe}/\text{H}]$. The black dots, track and shadowed area are the observations (sources listed in Table 1); dark blue line is model LC000+MRD; lighter blue lines are model LC000+NSM with variations in the time delay, namely (from darker to lighter) $\tau = 0, 1, 10, 100$ Myr (see Table 4).

models LC000+NSM and LC150+NSM with the non rotating and the 150 km/s data sets respectively (τ increases with lighter blue shades); in dark blue, models with MRD SNe. The conclusions are similar to the previous case: the best choice for NSMs is a time delay of 1 Myr, while with a coalescence time of $\tau = 0$ Myr the trend results very similar to the model where MRD SNe are used.

Finally, Figure 11 shows the models LC300+NSM with rotating 300 km/s Limongi & Chieffi (2018) yields. In this case, the higher velocity adopted produces trends that are not compatible with the abundances measured in Galactic halo stars. Concerning fast rotation, a variation of NSM coalescence timescale does not seem to affect the behaviour in any way: the trends for fastest speeds appear unaltered.

6 CONCLUSIONS

In this paper, the nucleosynthesis of neutron capture elements has been studied; we focused our attention on the production of the heavy elements barium and strontium. Stellar rotation has been taken into account: recent studies showed that it has a deep impact on stellar nucleosynthesis, enhancing heavy element production.

In this work, prescriptions from different authors have been tested and compared with the most recent observational data, in order to verify the differences and the similarities by means of a chemical evolution model. The results were compared with the observational data to verify which assumptions reproduced better the observations. We compared the prescriptions assumed for s-process component in rotating massive stars taken from Frischknecht et al. (2016) and from Limongi & Chieffi (2018), in which three different initial rotational speeds were considered. We also tested two possible sources of r-process material, namely NSMs, assum-

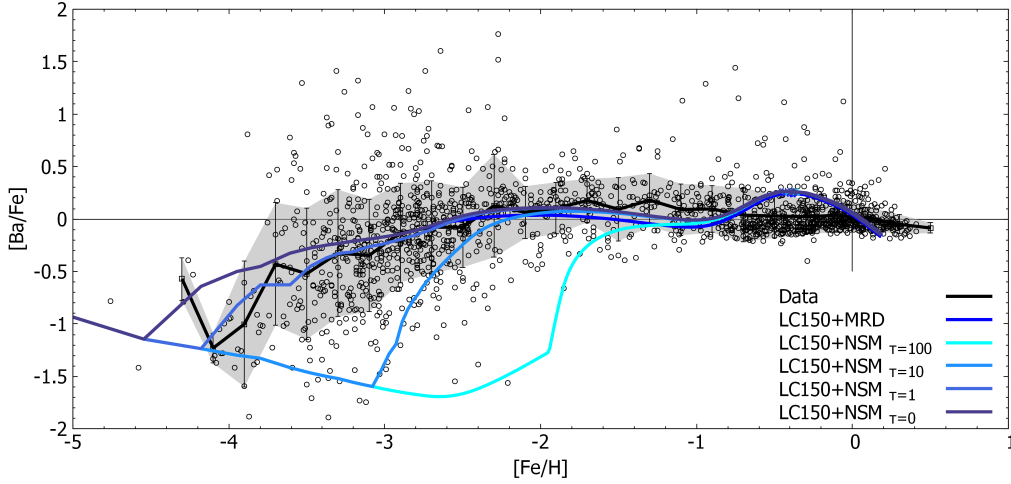


Figure 10. $[\text{Ba}/\text{Fe}]$ versus $[\text{Fe}/\text{H}]$. The black dots, track and shadowed area are the observations (sources listed in Table 1); dark blue line is model LC150+MRD; lighter blue lines are model LC150+NSM with variations in the time delay, namely (from darker to lighter) $\tau = 0, 1, 10, 100$ Myr (see Table 4).

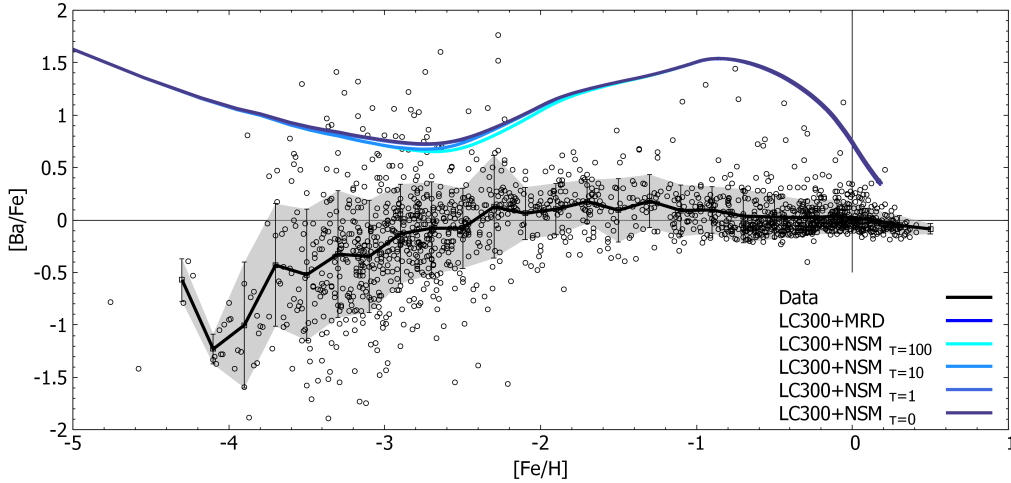


Figure 11. $[\text{Ba}/\text{Fe}]$ versus $[\text{Fe}/\text{H}]$. The black dots, track and shadowed area are the observations (sources listed in Table 1); dark blue line is model LC300+MRD; lighter blue lines are model LC300+NSM with variations in the time delay, namely (from darker to lighter) $\tau = 0, 1, 10, 100$ Myr (see Table 4).

ing the yields from [Matteucci et al. \(2014\)](#) and MRD SNe, using the prescriptions from [Cescutti & Chiappini \(2014\)](#). We summarize our conclusions as follows.

- The best fits to the data were the ones with the yield set of [Frischknecht et al. \(2016\)](#) or assuming all stars rotate with an initial velocity of 150 km/s from [Limongi & Chieffi \(2018\)](#).
- Although the non rotating models could explain the average trends of $[\text{Sr}/\text{Fe}]$ and $[\text{Ba}/\text{Fe}]$, so the pure production of r-process for these elements, they produce results non compatible for the $[\text{Sr}/\text{Ba}]$ ratio, proving that rotation is a necessary assumption to reproduce the actual behaviour of the observational data.
- Interpolations over the [Limongi & Chieffi \(2018\)](#) velocity sets have been calculated. The model assuming a velocity of 75 km/s has shown to produce results compatible with the data.
- Using the nucleosynthesis by [Limongi & Chieffi \(2018\)](#)

the best fit to the data could be obtained by assuming the slow rotating yields at the lowest metallicities and the non rotating yields for higher metallicities.

- The models with NSMs as r-process sources have been tested with a NSM time delay of 0, 1, 10 and 100 Myr. Both [Frischknecht et al. \(2016\)](#) and [Limongi & Chieffi \(2018\)](#) prescriptions for the low velocity set displayed an optimal behaviour with $\tau = 1$ Myr. The variation of the r-process site does not change our conclusions concerning the rotating massive stars.

We conclude that [Frischknecht et al. \(2016\)](#) assumption of different rotational velocity as function of metallicity is valid, since it is effective in reproducing the observations in every scenario.

On the other hand, we can use the nucleosynthesis by [Limongi & Chieffi \(2018\)](#), but different velocities should be adopted to fit at best the data; in particular assuming an initial velocity of 150 km/s at low metallicity and no rotation

or very low rotation above $[\text{Fe}/\text{H}] \sim -2$. A similar conclusion has been reached in [Prantzos et al. \(2018\)](#), studying the nitrogen production.

However, the comparison to [Prantzos et al. \(2018\)](#) is to be carefully considered: their work used [Limongi & Chieffi \(2018\)](#) yields for massive stars, but different assumptions were made. In particular, stars larger than $25 M_{\odot}$ fail to explode and always fall back into black holes, contributing to the chemical enrichment only through stellar winds. Furthermore, a direct observation of barium behaviour at low metallicities shows that [Prantzos et al. \(2018\)](#) employed a stronger s-process from rotating massive stars, for they assumed the average velocity to depend on metallicity, faster at low $[\text{Fe}/\text{H}]$, while in our framework Ba is mostly produced by r-process.

Our study of neutron star mergers have shown they are a good source for r-process: the best fit is obtained for a coalescence time of 1 Myr. The same conclusions have been achieved in the works of [Matteucci et al. \(2014\)](#) and [Cescutti et al. \(2015\)](#).

ACKNOWLEDGEMENTS

GC acknowledges financial support from the EU Horizon2020 programme under the Marie Skłodowska-Curie grant 664931. FM acknowledges funds from University of Trieste (Fondo per la Ricerca d'Ateneo - FRA2016). RH acknowledges support from the World Premier International Research Center Initiative (WPI Initiative), MEXT, Japan. GC and RH acknowledge support from the ChETEC COST Action (CA16117), supported by COST (European Cooperation in Science and Technology). This work has been partially supported by the Italian grants “Premiale 2015 MITiC” (P.I. B. Garilli) and “Premiale 2015 FIGARO” (P.I. G. Gemme).

REFERENCES

- Abbott B. P., et al., 2017, *Physical Review Letters*, **119**, 161101
- Aoki W., et al., 2002, *PASJ*, **54**, 427
- Aoki W., et al., 2005, *ApJ*, **632**, 611
- Aoki W., Honda S., Sadakane K., Arimoto N., 2007a, *PASJ*, **59**, L15
- Aoki W., Beers T. C., Christlieb N., Norris J. E., Ryan S. G., Tsangarides S., 2007b, *ApJ*, **655**, 492
- Aoki W., et al., 2008, *ApJ*, **678**, 1351
- Aoki W., Ito H., Tajitsu A., 2012, *ApJ*, **751**, L6
- Aoki W., et al., 2013, *AJ*, **145**, 13
- Aoki W., Tominaga N., Beers T. C., Honda S., Lee Y. S., 2014, *Science*, **345**, 912
- Arcones A., Janka H.-T., Scheck L., 2007, *A&A*, **467**, 1227
- Argast D., Samland M., Thielemann F.-K., Qian Y.-Z., 2004, *A&A*, **416**, 997
- Asplund M., Grevesse N., Sauval A. J., Scott P., 2009, *ARA&A*, **47**, 481
- Barklem P. S., et al., 2005, *A&A*, **439**, 129
- Battistini C., Bensby T., 2016, *A&A*, **586**, A49
- Bensby T., et al., 2011, *A&A*, **533**, 134
- Bensby T., Feltzing S., Oey M. S., 2014, *A&A*, **562**, A71
- Bonifacio P., et al., 2009, *A&A*, **501**, 519
- Burbidge E. M., Burbidge G. R., Fowler W. A., Hoyle F., 1957, *Rev. Mod. Phys.*, **29**, 547
- Burris D. L., Pilachowski C. A., Armandroff T. E., Sneden C., Cowan J. J., Roe H., 2000, *ApJ*, **544**, 302
- Caffau E., et al., 2011, *Msngr*, **146**, 28
- Carretta E., Gratton R., Cohen J. G., Beers T. C., Christlieb N., 2002, *AJ*, **124**, 481
- Caughlan G. R., Fowler W. A., 1988, *At. Data Nucl. Data Tables*, **40**, 283
- Cayrel R., et al., 2004, *A&A*, **416**, 1117
- Cescutti G., Chiappini C., 2014, *A&A*, **565**, A51
- Cescutti G., François P., Matteucci F., Cayrel R., Spite M., 2006, *A&A*, **448**, 557
- Cescutti G., Chiappini C., Hirschi R., Meynet G., Frischknecht U., 2013, *A&A*, **553**, A51
- Cescutti G., Romano D., Matteucci F., Chiappini C., Hirschi R., 2015, *A&A*, **577**, 139
- Cescutti G., Valentini M., François P., Chiappini C., Depagne E., Christlieb N., Cortés C., 2016, *A&A*, **595**, A91
- Chiappini C., Matteucci F., Gratton R., 1997, *ApJ*, **477**, 765
- Chieffi A., Limongi M., 2013, *ApJ*, **764**, 21
- Christlieb N., Gustafsson B., Korn A. J., Barklem P. S., Beers T. C., Bessell M. S., Karlsson T., Mizuno-Wiedner M., 2004, *ApJ*, **603**, 708
- Cohen J. G., et al., 2004, *ApJ*, **612**, 1107
- Cohen J. G., Christlieb N., Thompson I., McWilliam A., Shectman S., Reimers D., Wisotzki L., Kirby E., 2013, *ApJ*, **778**, 56
- Côté B., et al., 2018, arXiv e-prints,
- Cowan J. J., Thielemann F.-K., Truran J. W., 1991, *Phys. Rep.*, **208**, 267
- Cowan J. J., et al., 2002, *ApJ*, **572**, 861
- Cristallo S., Straniero O., Gallino R., Piersanti L., Domínguez I., Lederer M. T., 2009, *ApJ*, **696**, 797
- Cristallo S., et al., 2011, *ApJS*, **197**, 17
- Frebel A., Christlieb N., Norris J. E., Thom C., Beers T. C., Rhee J., 2007, *ApJL*, **660**, L117
- Frischknecht U., Hirschi R., Thielemann F.-K., 2012, *A&A*, **538**, L2
- Frischknecht U., et al., 2016, *MNRAS*, **456**, 1803
- Fulbright J. P., 2000, *AJ*, **120**, 1841
- Hansen C. J., et al., 2012, *A&A*, **545**, A31
- Hansen T., et al., 2015, *ApJ*, **807**, 173
- Hayek W., et al., 2009, *A&A*, **504**, 511
- Hirschi R., 2007, *A&A*, **461**, 571
- Hollek J. K., Frebel A., Roederer I. U., Sneden C., Shetrone M., Beers T. C., Kang S. J., Thom C., 2011, *ApJ*, **742**, 54
- Honda S., Aoki W., Kajino T., Ando H., Beers T. C., Izumiura H., Sadakane K., Takada-Hidai M., 2004, *ApJ*, **607**, 474
- Honda S., Aoki W., Beers T. C., Takada-Hidai M., 2011, *ApJ*, **730**, 77
- Ishigaki M., Chiba M., Aoki W., 2010, *PASJ*, **62**, 143
- Ishigaki M. N., Aoki W., Chiba M., 2013, *ApJ*, **771**, 67
- Ivans I. I., Sneden C., James C. R., Preston G. W., Fulbright J. P., Höfflich P. A., Carney B. W., Wheeler J. C., 2003, *ApJ*, **592**, 906
- Ivans I. I., Simmerer J., Sneden C., Lawler J. E., Cowan J. J., Gallino R., Bisterzo S., 2006, *ApJ*, **645**, 613
- Jacobson H. R., et al., 2015, *ApJ*, **807**, 171
- Johnson J. A., 2002, *ApJS*, **139**, 219
- Jonsell K., Edvardsson B., Gustafsson B., Magain P., Nissen P. E., Asplund M., 2005, *A&A*, **440**, 321
- Kalogera V., et al., 2004, *ApJ*, **614**, L137
- Karakas A.-I., 2010, *ASSP*, **16**, 107
- Kobayashi C., Umeda H., Nomoto K., Tominaga N., Ohkubo T., 2006, *ApJ*, **653**, 1145
- Lai D. K., Johnson J. A., Bolte M., Lucatello S., 2007, *ApJ*, **667**, 1185
- Lai D. K., Bolte M., Johnson J. A., Lucatello S., Heger A., Woosley S. E., 2008, *ApJ*, **681**, 1524

- Li H., Aoki W., Zhao G., Honda S., Christlieb N., Suda T., 2015a, *PASJ*, 67, 84
- Li H. N., Zhao G., Christlieb N., Wang L., Wang W., Zhang Y., Hou Y., Yuan H., 2015b, *ApJ*, 798, 110
- Limongi M., Chieffi A., 2003, *ApJ*, 592, 404
- Limongi M., Chieffi A., 2018, *ApJS*, 237, 13
- Mashonkina L., Christlieb N., Barklem P. S., Hill V., Beers T. C., Velichko A., 2010, *A&A*, 516, A46
- Mashonkina L., Christlieb N., Eriksson K., 2014, *A&A*, 569, A43
- Masseron T., et al., 2006, *A&A*, 455, 1059
- Masseron T., Johnson J. A., Lucatello S., Karakas A., Plez B., Beers T. C., Christlieb N., 2012, *ApJ*, 751, 14
- Matteucci F., Recchi S., 2001, *ApJ*, 558, 351
- Matteucci F., Romano D., Arcones A., Korobkin O., Rosswog S., 2014, *MNRAS*, 438, 2177
- Matteucci F., Romano D., Cescutti G., Simonetti P., 2018, *Rendiconti Lincei*, submitted
- McWilliam A., Preston G. W., Sneden C., Searle L., 1995, *AJ*, 109, 2757
- Meynet G., Maeder A., 2002, *A&A*, 390, 561
- Meynet G., Ekström S., Maeder A., 2006, *A&A*, 447, 623
- Nishimura N., Takiwaki T., Thielemann F.-K., 2015, *ApJ*, 810, 109
- Norris J. E., Ryan S. G., Beers T. C., Deliyannis C. P., 1997a, *ApJ*, 485, 370
- Norris J. E., Ryan S. G., Beers T. C., 1997b, *ApJ*, 488, 350
- Norris J. E., Ryan S. G., Beers T. C., 1997c, *ApJ*, 489, L169
- Placco V. M., Frebel A., Beers T. C., Christlieb N., Lee Y. S., Kennedy C. R., Rossi S., Santucci R. M., 2014, *ApJ*, 781, 40
- Placco V. M., Frebel A., Lee Y. S., Jacobson H. R., Beers T. C., Pena J. M., Chan C., Heger A., 2015, *ApJ*, 809, 136
- Prantzos N., Abia C., Limongi M., Chieffi A., Cristallo S., 2018, *MNRAS*, 476, 3432
- Preston G. W., Sneden C., 2000, *AJ*, 120, 1014
- Preston G. W., Thompson I. B., Sneden C., Stachowski G., Shectman S. A., 2006, *AJ*, 132, 1714
- Raiteri C. M., Gallino R., Busso M., 1992, *ApJ*, 387, 263
- Roederer I. U., Sneden C., Thompson I. B., Preston G. W., Shectman S. A., 2010, *ApJ*, 711, 573
- Roederer I. U., Jacobson H. R., Thanathibodee T., Frebel A., Toller E., 2014, *ApJ*, 797, 69
- Rosswog S., Liebendörfer M., Thielemann F.-K., Davies M. B., Benz W., Piran T., 1999, *A&A*, 341, 499
- Ryan S. G., Norris J. E., Bessell M. S., 1991, *AJ*, 102, 303
- Ryan S. G., Norris J. E., Beers T. C., 1996, *ApJ*, 471, 254
- Scalo J. M., 1986, *Fund. Cosmic Phys.*, 11, 1
- Simmerer J., Sneden C., Cowan J. J., Collier J., Woolf V. M., Lawler J. E., 2004, *ApJ*, 617, 1091
- Simonetti P., Matteucci F., Greggio L., Cescutti G., 2019, arXiv e-prints,
- Siqueira Mello C., et al., 2014, *A&A*, 565, A93
- Spite M., Spite F., Bonifacio P., Caffau E., François P., Sbordone L., 2014, *A&A*, 571, A40
- Travaglio C., Galli D., Gallino R., Busso M., Ferrini F., Straniero O., 1999, *ApJ*, 521, 691
- Travaglio C., Gallino R., Arnone E., Cowan J., Jordan F., Sneden C., 2004, *ApJ*, 601, 864
- Truran J. W., 1981, *A&A*, 97, 391
- Westin J., Sneden C., Gustafsson B., Cowan J. J., 2000, *ApJ*, 530, 783
- Winteler C., Käppeli R., Perego A., Arcones A., Vasset N., Nishimura N., Liebendörfer M., Thielemann F.-K., 2012, *ApJ*, 750, L22
- Yong D., et al., 2013, *ApJ*, 762, 26
- Zhang L., Ishigaki M., Aoki W., Zhao G., Chiba M., 2009, *ApJ*, 706, 1095

This paper has been typeset from a $\text{\TeX}/\text{\LaTeX}$ file prepared by the author.